Journal of Environmental Chemical Engineering 5 (2017) 147–159

Contents lists available at ScienceDirect

Journal of Environmental Chemical Engineering

journal homepage: www.elsevier.com/locate/jece

Research Paper

Adsorptive desulphurization of model oil by Ag nanoparticles-modified activated carbon prepared from brewer's spent grains

A.A. Olajire[a,*], J.J. Abidemi[b], A. Lateef[c], N.U. Benson[d]

[a] Department of Pure and Applied Chemistry, Ladoke Akintola University of Technology, Ogbomoso, Nigeria
[b] Afe Babalola University, Ado-Ekiti, Ekiti, Nigeria
[c] Department of Pure and Applied Biology,Ladoke Akintola University of Technology, Ogbomoso, Nigeria
[d] Environmental Chemistry Unit, Department of Chemistry, Covenant University, Ota, Nigeria

ARTICLE INFO

Article history:
Received 28 July 2016
Received in revised form 19 November 2016
Accepted 24 November 2016
Available online 25 November 2016

Keywords:
Desulphurization
Adsorption
Ag nanoparticles
Dibenzothiophene
Activated carbon

ABSTRACT

This study reports removal of dibenzothiophene (DBT) from model oil (DBT dissolved in *n*-heptane) by silver nanoparticles modified activated carbon prepared from brewer's spent grains using wet impregnation (WI) method. The removal efficiency follows the order $AgNPs^{cw}/AC > AgNPs^{kp}/AC >$ ACB. The $AgNPs^{kp}$/AC and $AgNPs^{cw}$/AC exhibit higher adsorption capacities for DBT with maximum values of 25.7 and 29.8 mg $_{DBT}/g_{Ads}$ at 25 °C respectively, than ACB with 13.9 mg $_{DBT}/g_{Ads.}$ The two-fold enhancement in the DBT uptake capacities of modified ACs can be attributed to the introduction of Ag(1) ion, a weak Lewis acid as an additional adsorption site. A significant decrease from 212.9 to 136.2 m^2/g in the Brunauer–Emmett–Teller surface area of $AgNPs^{cw}$/AC is observed following the loading of DBT. The equilibrium adsorption data is adequately represented by Freundlich isotherm. The adsorption kinetics of DBT by these adsorbents followed pseudo second-order (PSO) model and the mechanism of adsorption was controlled by film and intra-particle diffusion. The change in entropy and heat of adsorption for DBT adsorption by these adsorbents range from 0.18 to 0.19 kJ/mol K and 21.5 to 23.9 kJ/mol, respectively. The results indicate that Ag nanoparticles-modified ACs from brewer's spent grains can be used as adsorbent for the removal of DBT from model oil.

1. Introduction

In recent times, growing concerns regarding the air quality and associated deleterious effects to the environment posed by gasoline and diesel oil combustion process may have necessitated the removal of heteroatomic components from crude oil by petroleum refining industries in order to produce cleaner and environmental friendly products [81]. Many conventional approaches of desulfurization geared towards improving the removal efficiency of sulphur compounds from crude oil have been developed and reported in the literature [14,65,49]. Some of these technologies could address key questions surrounding emission quality and pollution. The current desulfurization technology in petroleum industry is heterogeneously catalyzed hydrodesulfurization (HDS). The inherent chemical limitations associated with HDS coupled with high cost make alternatives to this technology of interest attractive to the petroleum industry. Various types of techniques have been developed to reduce or remove sulphur compounds by oxidation [20,29,38], extraction [39,66], adsorption [7,54,68,84] and biodesulphurization [28].

Adsorption constitutes an attractive alternative to HDS method and is commonly employed in removing sulphur compounds from diesel oil [62,75]. Various researchers have used adsorption processes to remove sulphur compounds from fuels using different types of adsorbents [37,43,52,60,76]. Activated carbons (ACs) have been extensively studied because of their high surface area, cost effectiveness, receptivity to modification and high affinity for sulfur compounds removal from different fuels [10,16,82,86].

In the past few years, nanoparticles-modified adsorbents have attracted much interest due to high surface area to volume ratio and short diffusion rate [74,85,77]. Most previous applications of nanoparticles-modified sorbents were mainly focused on removal of dyes and heavy metal ions from environmental water samples [15,56,63,55]. However, reports on the removal of sulfur compounds from model oil by Ag nanoparticles-modified AC prepared from Brewer's spent grain (BSG) is sparse [13,36,6,42,27]. The generation of ACs from BSG is an appealing method that gives increased values to this material, which is principally utilized as

* Corresponding author.
E-mail address: olajireaa@yahoo.com (A.A. Olajire).

http://dx.doi.org/10.1016/j.jece.2016.11.033
2213-3437/

animal feeding. AgNPs have been successfully synthesized using seed shell extract and novel biomaterial (cobweb). The synthetic method employed in this study is green and non hazardous to the environment.

In the present study, Ag nanoparticles-modified AC has been explored as an alternative method for desulfurization of model oil. Silver nanoparticles was chosen for sorbent modification because of its high activity, which has been suggested to be due to release of Ag^0 (atomic) and Ag^+ (ionic) clusters on dissolution, where the Ag^+ can form complex with electron donor groups containing sulfur such as DBT [17]. We therefore explored the strong affinity of Ag for sulphur containing compounds to synthesize Ag nanoparticles-modified ACs for subsequent applications to single component adsorption of DBT in *n*-heptane, in order to provide fundamental understanding and the effect of adsorbent modification on the removal of DBT from model oil.

2. Materials and methods

2.1. Materials

2.1.1. Adsorbent preparation

The brewer's spent grains (BSG) were supplied by the Nigerian Breweries. The material was washed with water to remove residues from wort and dried in the sun for 6 h until approximately 10% moisture content. Dried BSG was then placed in an oven maintained at 105 °C to completely eliminate the moisture. Thereafter, 10 g of moisture-free BSG was weighed in a crucible (50 mm diameter) and carbonized at 300 °C, at initial heating rate of 20 °C/min for 30 min in a muffle furnace (Carbolic Sheffied England LF4) and cooled at room temperature [1].

Precisely 5.0 g of sieved (10 μm mesh) carbonized BSG was activated by treatment with 5.0 mL of 0.3 M H_3PO_4

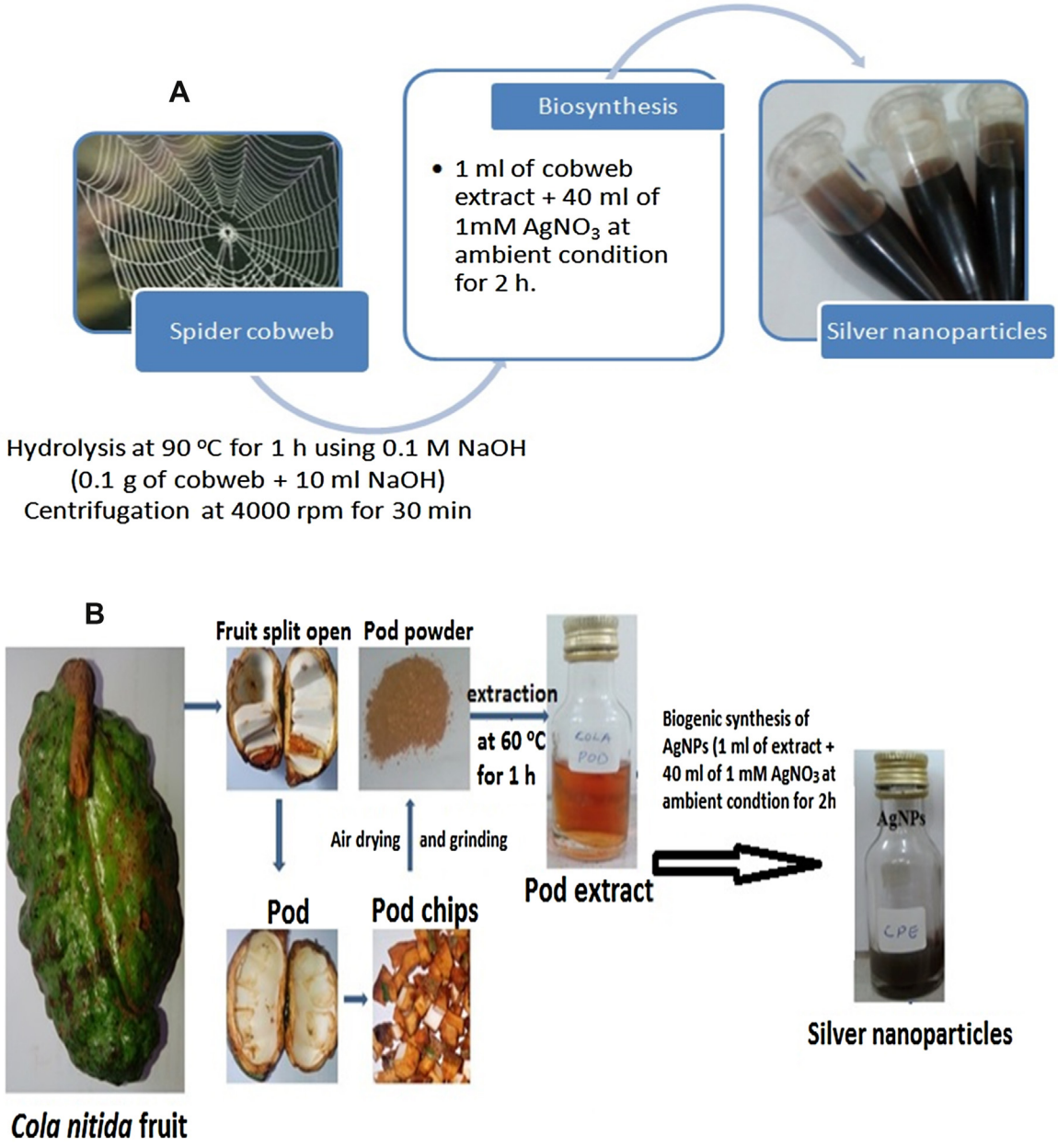

Fig. 1. Scheme for the synthesis of silver nanoparticles from cobweb (A) and *Cola nitida* fruit (B).

(1M = 1moldm^{-3}) and left for an impregnation time of 1 h at room temperature to form a paste. After this time, the blend was transferred to a muffle furnace, where carbonization was carried out at 300 °C under air atmosphere. The furnace was heated at 20 °C/min up to 300 °C, and maintained at this temperature for 1 h to allow the free evolution of water, obtaining a black sticky solid. After cooling to room temperature, the solid was washed with distilled water to remove excess H_3PO_4 [71]. The activated carbon samples were oven dried at 105 °C to a constant weight and kept in air tight vial as acid activated carbon (ACB).

2.1.2. Green synthesis of silver nanoparticles

The AgNPs were synthesized from Cobwebs (*AgNPs^{cw}*) and *Cola nitida* plant(*AgNPs^{kp}*) [46,47]. About 0.1 g of cobwebs was weighed and hydrolyzed with 10 mL of 0.1 M NaOH at 90 °C for 1 h. The hydrolyzed cobweb was allowed to cool and centrifuged at 4000 rpm for 30 min. Approximately 1 mL of cobweb extract was added to reaction vessel containing 40 mL of 1 mM silver nitrate solution ($AgNO_3$) for the reduction of silver ion. The reaction was carried out at laboratory temperature (25.0 °C ± 0.1 °C) for 2 h with formation of silver nanoparticles (*AgNPs^{cw}*) that is dark brown in color with maximum absorbance at the wavelength of 436 nm. The size of the silver nanoparticles as determined from TEM analysis ranged from 3 to 50 nm with average particle size of 25 ± 18 nm.

Similarly, the extracts of seed shell of *Cola nitida* were obtained by heating one gram in water bath at 60 °C for 1 h and filterated to obtain the extract. Approximately, 1 mL of the extract was added to 40 mL of 1 mM $AgNO_3$ solution in the reaction vessel, for the reduction of silver ion. The biosynthesized silver nanoparticles (*AgNPs^{kp}*) depicted yellowish orange with maximum absorbance reading at 454.5 nm. The size of the silver nanoparticles as determined from TEM analysis ranged from 12 to 80 nm with average particle size of 43 ± 25 nm. Fig. 1 shows the scheme for synthesis of silver nanoparticles from cobwebs and *Cola nitida* plant.

2.1.3. Loading of silver nanoparticles on activated carbon

Precisely 100 mL of the freshly prepared Ag nanoparticles solution (0.170 mg/L) was mixed with 5.0 g of AC in a 250 mL Erlenmeyer flask under magnetic stirring at laboratory temperature overnight to ensure complete coating. After deposition of the Ag nanoparticles onto AC, the Ag nanoparticles-modified AC mixture was filterated and dried at 110 °C in an oven for 10 h to give 3.4×10^{-3} mg of AgNPs/g AC (labeled as *AgNPs^{cw}/ACandAgNPs^{kp}/AC*).

2.2. Adsorbent characterization

The functional groups on the adsorbents were characterized by Fourier transform infrared spectrophotometer (PerkinElmer Spectrum 100 series FT-IR Spectrometer, USA) in the range of 400–4000 cm^{-1}. The adsorbents' textures and morphologies were studied using high resolution transmission electron microscope (HRTEM) coupled with Energy dispersive X-ray spectroscopy (EDX) Oxford detector (model X-Max. A JOEL-2100F, USA).The crystalline structures in the adsorbents were studied with powder X-ray diffraction (Bruker D2, Phaser DOC-M88-EXX, 155 V4-07, Germany). XRD analysis was done using Cu-Kα as a source and Ni as a filter media, and K radiation maintained at 1.5418 Å. The XRD data were recorded for 2θ values between 10° and 90°. The crystalline phases were identified by comparison with the reference data from the International Center for Diffraction Data (ICDD) database.

Textural characteristics of the adsorbents were determined by N_2 adsorption at 77.15 K using an automatic Micrometritics Instrument Corporation 2012, TriStar 11, 3020, USA.

2.3. Adsorbate

All the chemicals used in the study were of analytical reagent (AR) grade. Dibenzothiophene ($C_{12}H_8S$, 184.3 g/mol) with 99.9% purity and *n*-heptane were procured from Sigma Aldrich. Stock solution of sulfur having 1 g/L concentration was made by dissolving 5.758 g of DBT in 1000 mL *n*-heptane. The range of concentration of sulfur solutions were prepared from stock solution by diluting with *n*-heptane.

2.4. Adsorption experiment

The adsorption of DBT on activated carbon (AC) and Ag nanoparticles modified AC was performed at a constant shaking rate of 120 rpm in a temperature control water bath shaker (SearchTech Instrument SHZ-82, India) maintained at 25.0 °C ± 0.1 °C except for the experiments carried out to test the effect of temperature using a batch mode experiment. For adsorption isotherms study, solutions of DBT at concentrations of 100, 200, 300, 400, 500 and 600 mg/L in 50 mL *n*-heptane as a model oil were each used with 300 mg of adsorbent and contact time of 100 min. To study the adsorption kinetics on the adsorbents, a 50 mL model oil solution with an initial concentration of 100 mg/L DBT was added to 200 mg of the adsorbent in a vial that was capped and then shaken continuously for a fixed time intervals. The adsorbent was then allowed to settle and filterated for determination of residual DBT concentration. The same procedure was carried out for shaking time intervals of 10, 20, 30, 40, 60, 70, 80, 90 and 100 min. The effect of the adsorbent amount on the removal of DBT with initial concentration of 400 mg/L was studied by varying the adsorbent mass from 100 to 500 mg. The residual concentration of the DBT in model oil was analyzed for the absorbance by using UV/visible spectrophotometer (Model 752, Gallenkomp, UK) at wavelength of 325 nm. The residual concentration of the DBT in model oil was calculated from the absorbance using the calibration curve (Fig. 2) prepared by taken absorbance (A) readings in triplicates at 325 nm of various concentrations of DBT solutions. The calibration curve was found to be linear up to 140 mg/L of DBT with $R^2 \cong 0.99$. The ΔA values for DBT determination are low enough (<5% of the mean) to assume a good mathematical fit. The DBT adsorbed per unit mass of the adsorbent (mg/g), and percentage adsorption were calculated using Eqs. (1) and (2).

$$q_e = \frac{(C_o - C_e)V}{m} \quad (1)$$

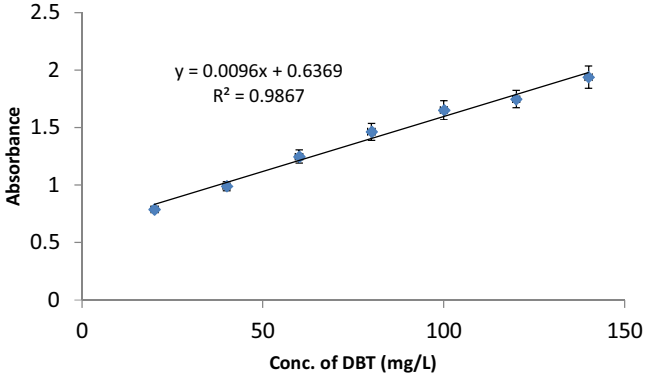

Fig. 2. Calibration plot with error bars of model sulphur compound.

$$\text{Percentagesulphurremoval} = \frac{100(C_o - C_e)}{C_o} \quad (2)$$

where, C_o is the initial DBT concentration ($mg_{DBT}/L_{modeloil}$), C_e is the remaining concentration of DBT in model oil at equilibrium ($mg_{DBT}/L_{modeloil}$), V is the volume of model oil in litre and m is the mass of the adsorbent in gram.

2.5. Adsorption isotherm studies

Here, we established the most appropriate correlation for the equilibrium isotherm curves. We used three isotherm models namely Langmuir [45], Freundlich [24] and Temkin [73] to fit the experimental data for the adsorption of DBT from model oil onto the adsorbents at 298 K.

2.6. Batch kinetic studies

The adsorption kinetics of DBT onto adsorbent was investigated using pseudo-first-order (PFO) model, expressed [44] as:

$$q_t = q_e(1 - e^{-k_1 t}) \quad (3)$$

where k_1 is pseudo-first-order rate constant.

The pseudo-second-order (PSO) model is represented as given by [34],

$$q_t = \frac{k_2 q_e^2 t}{(1 + k_2 q_e t)} \quad (4)$$

where k_2 (g/mg min) is the pseudo second-order rate constant.

The Elovich equation is simply expressed [5] as:

$$\frac{dq_t}{dt} = \alpha e^{(-\beta q_t)} \quad (5)$$

where α is the initial desorption rate (mg/(g min)) and β is the desorption constant (g/mg) during any experiments.

2.7. Validity of the models

The R^2 values and normalized standard deviation, $\Delta q_t(\%)$ were used to verify the most suitable kinetics and isotherm model to describe the adsorption process. It is defined as:

$$\Delta q_t(\%) = 100\sqrt{\frac{1}{n-1}\left(\sum_{i=1}^{i=n}\left(\frac{q_{e,i,\text{exp}} - q_{e,i,cal}}{q_{e,i,\text{exp}}}\right)^2\right)} \quad (6)$$

Where n is the number of data points, q_{exp} and q_{cal} (mg_{DBT}/g_{Ads}) are the experimental and calculated adsorption capacity values. Lower value of Δq_t indicates close agreement between experimental and calculated data.

2.8. Adsorption thermodynamics

The experimental data obtained from batch adsorption studies were analyzed by using the following thermodynamic equations:

$$\Delta G = -RTInK_L \quad (7)$$

Where R is the universal gas constant, 8.314 J/mol K^{-1}; T is the temperature in Kelvin; and K_L is the Langmuir equilibrium constant in L/mg, defined as;

$$K_L = \frac{q_e}{C_e} \quad (8)$$

It is well known that the unit for ΔG is in J/mol and the term RT is also J/mol, then the equilibrium constant K_L in equation (7) must be dimensionless. In order to obtain correct value of ΔG, thus correct interpretation of ΔS and ΔH, the K_L value in Eq. (7) must be dimensionless [53]. Therefore K_L was recalculated as dimensionless quantity by multiplying it by 6.795×10^5 mg/L of n-heptane solution (from the density of n-heptane solution of 0.6795 g/mL).

$$\therefore \Delta G = -RTIn6.795x10^5 K_L$$
$$\Delta G = -RTInK_L^r \quad (9)$$

where K_L^r is the recalculated K_L.

But,

$$\Delta G = \Delta H - T\Delta S \quad (10)$$

$$\therefore InK_L^r = \frac{\Delta S}{R} - \frac{\Delta H}{RT} \quad (11)$$

ΔG was calculated using Eq. (10). The values of ΔH and ΔS were obtained respectively from the slope and intercept of Van't Hoff plot of InK_L^r versus $1/T$. Values of K_L were calculated from Eq. (8) at different solution temperatures of 35 °C, 45 °C and55 °C.

2.9. Adsorption mechanism

The intra-particle diffusion was explored by using intra-particle diffusion model [78]:

$$q_t = k_{id}t^{1/2} + C_i \quad (12)$$

where C_i is the intercept and k_{id} (mg/g $min^{1/2}$) is the intra-particle diffusion rate constant.

2.10. Qualitative analysis of commercial gasoline with GC-PFPD

A Hewlett Packard 6890 gas chromatograph with a capillary column (DB-5, 30 m × 0.25 mm i.d. × 0.25 μm film thickness) and a split mode injector (ratio: 20:1) was used with ultrahigh-purity helium as a carrier gas. The injector temperature was kept at 250 °C. A plus flame photometric detector (PFPD, O.I. Analytical 5380) was used for identification and qualification of the commercial gasoline sample. For analysis of the gasoline sample, the column temperature program was set at 40 °C for 1 min, 4 °C/min from 40 until 280 °C and remained for 5 min, with injection volume of 1 μL. The detector temperature was 320 °C, while hydrogen pressure and compressed air were 20 psi and 35 psi respectively.

3. Results and discussion

3.1. Adsorbent characterization

3.1.1. Surface area and pore characteristics

The Brunauer–Emmett–Teller (BET) surface area, micropore volume(V_{mic}), total pore volume (V_{total}) and average pore diameter of the adsorbents are shown in Table 1. The surface area of ACB was 411.7 m^2/g with high pore volume of 0.54 cm^3/g. The average pore diameter is 13.2 nm. Upon surface modification with Ag

Table 1
Structural property of adsorbents determined by N_2 adsorption.

Sorbent	S_{BET} (m^2/g)	V_{total} (cm^3/g)	V_{mic} (cm^3/g)	Average pore diameter (nm)
ACB	412	0.54	0.52	13
$AgNPs^{kp}$/AC	215	0.37	0.35	19
$AgNPs^{cw}$/AC	213	0.34	0.33	21
$AgNPs^{cw}$/AC/DBT	136	0.22	0.21	127

nanoparticles, a high reduction in S_{BET}, V_{total} and V_{mic} with an increase in pore diameter of blank ACB was observed. The reduction in V_{mic} indicates that Ag nanoparticles are accumulated in micropores resulting in reductions in S_{BET} and V_{total}. Adsorbents of pore diameter range of 0.7–1.0 nm have been reported to be suitable for accessing DBT and other cyclic organosulphur compound (OSC), because the diameters of these compounds are comparable to the dimension of these adsorbents [16,67]. As indicated in Table 1, pore diameter of ACB has been increased after surface modification; however, pore diameter of all adsorbents is larger than 0.7 nm, which is necessary for accessing DBT inside the adsorbent [10,67]. Also, according to IUPAC classification [35], all the adsorbents belong to the mesopore region, which is suitable for adsorption of DBT from model oil.

Presence of DBT on the surface of AgNPs^{cw}/AC was confirmed by comparing the structural property of blank AgNPs^{cw}/AC with that of DBT loaded AgNPs^{cw}/AC. The BET surface areas of blank and DBT loaded AgNPs^{cw}/AC are found to be 212.9 and 136.2 m^2/g, respectively. The corresponding total pore volumes and average pore diameters are 0.34 and 0.22 cm^3/g; 21.0 and 127.5 m, respectively. The decrease in S_{BET} and V_{total} with increase in average pore diameter of AgNPs^{cw}/AC is due to the interaction that exists between DBT and Ag nanoparticles; and the hydrophobic interaction of *n*-heptane on the adsorbent surface.

3.1.2. Surface chemistry

The surface chemistry of the adsorbent was carried out with Fourier Transform infrared spectroscopic (FTIR) analysis of the ACB and Ag nanoparticles-modified AC samples (Fig. 3). The spectrum of the samples shows the presence of several functional groups. These spectra revealed either a reduction, appearance, disappearance or broadening of the peaks after the process of impregnation with Ag nanoparticles. The bands appearing at 1583 and 1586 cm^{-1} are ascribed to formation of oxygen functional groups like highly conjugated C=O stretching of carboxylic acid, lactone and quinines. The peaks at 1092 cm^{-1} are due to —OCH_3 group, which confirm the presence of the lignin structure [26], which were found in all the adsorbents. Upon surface modification, there are appearances of some additional peaks at 3059 cm^{-1} (AgNPs^{kp}/AC) and 2923 cm^{-1} (AgNPs^{cw}/AC), which can be attributed to stretching vibration of C—H, while other additional peaks at 773–460 cm^{-1} can be due C—H out of plane bending vibration.

Presence of DBT on the surface of AgNPs^{cw}/AC was confirmed by comparing the FTIR of blank AgNPs^{cw}/AC with that of DBT loaded AgNPs^{cw}/AC. It was observed that the peak at 1586 cm^{-1} for blank AgNPs^{cw}/AC shifted to a more intense peak at 1576 cm^{-1} for DBT loaded AgNPs^{cw}/AC, with disappearance of peak at 535 cm^{-1}. The peak at 1576 cm^{-1} could be due to C=C stretching vibration of thiophene.

3.1.3. Surface morphology/elemental composition

The morphological study of the prepared adsorbents was carried out with high resolution transmission spectroscopy (HRTEM) in order to check its surface and porosity. Generally the adsorbent with porous and rough morphology has high adsorption capacity [69,11]. Fig. 4 shows the HRTEM images of ACB, AgNPs^{kp}/AC, AgNPs^{cw}/AC and DBT-loaded AgNPs^{cw}/AC. From these micrographs, pores and finger-like structures are evident on the surface of the prepared adsorbents. The images show that all the adsorbents were rough and uneven. The surface of Ag

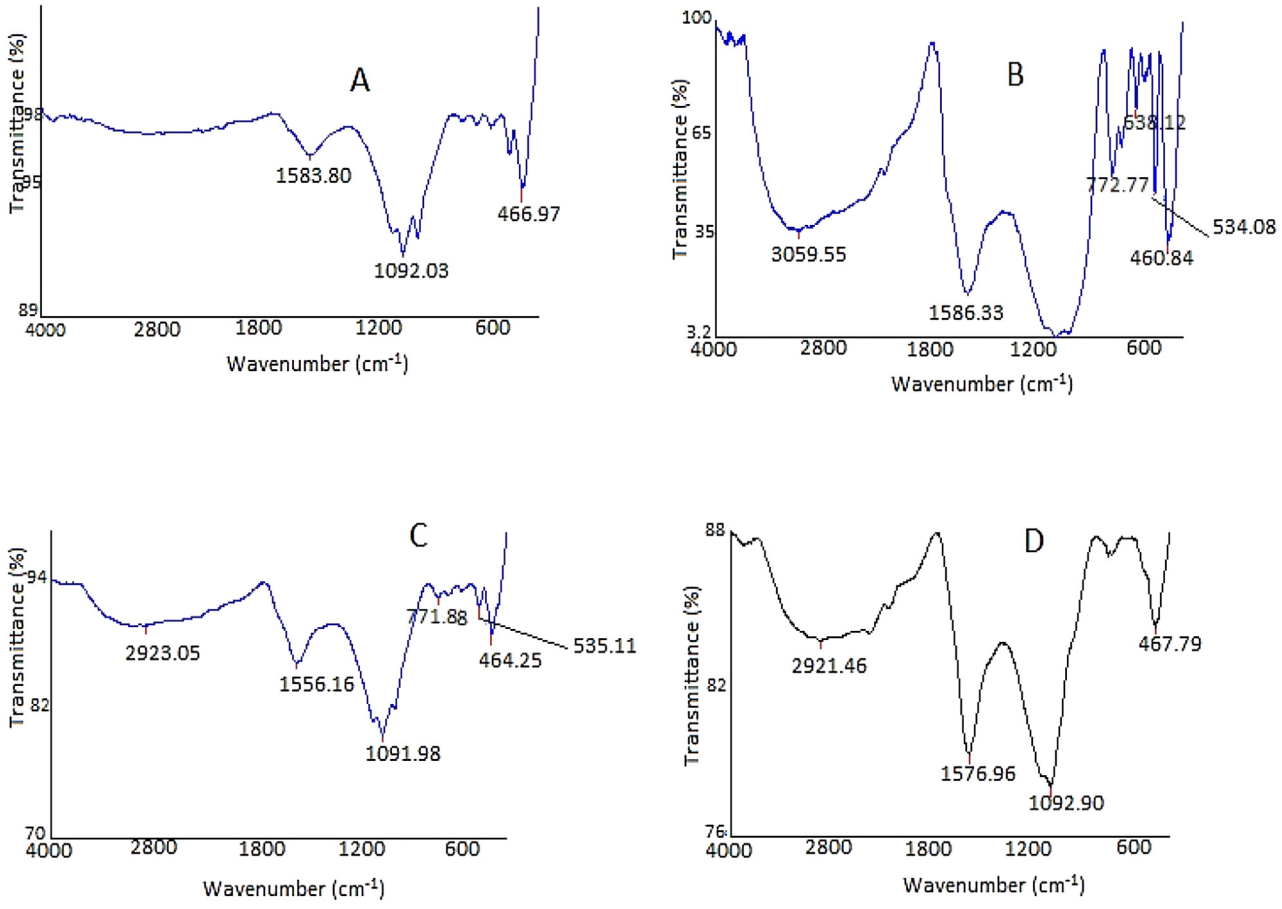

Fig. 3. FTIR spectra of (A) ACB, (B) AgNPs^{kp}/AC, (C) AgNP^{cw}/AC and (D) AgNPs^{cw}/AC/DBT.

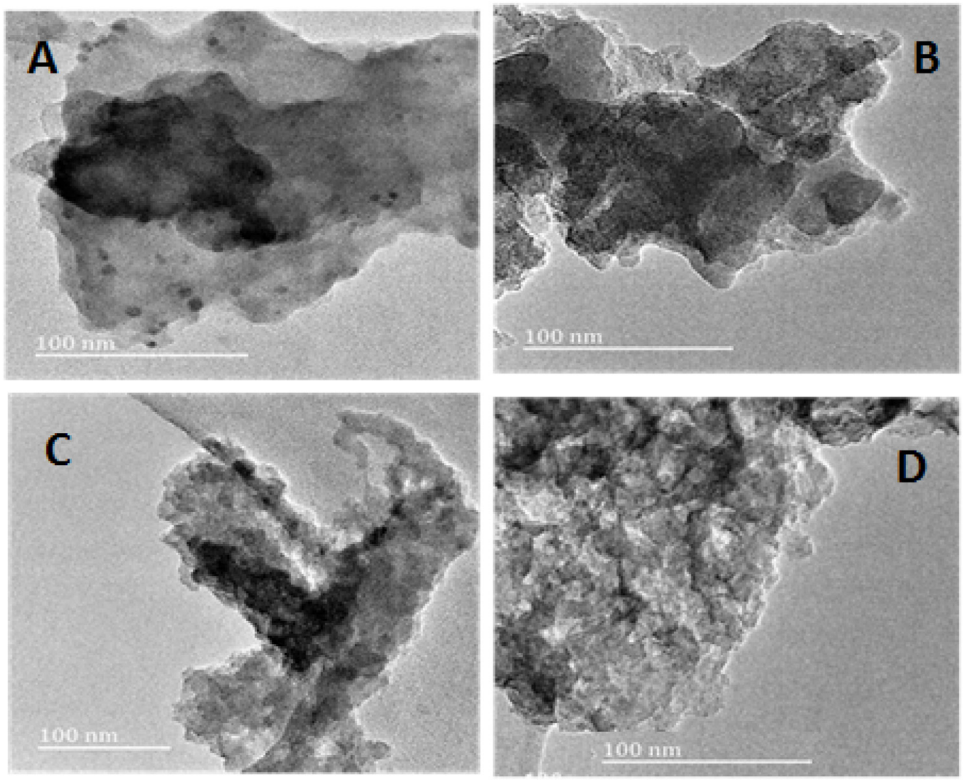

Fig. 4. HRTEM images of (A) ACB, (B) AgNPs^{kp}/AC, (C) AgNPs^{cw}/AC and (D) DBT-loaded AgNPs^{cw}/AC.

nanoparticles-modified ACs seems to be rougher with quite different shape from that of the blank ACB, which thus make them to have higher adsorption capacity than blank ACB. Pores that are present on the adsorbent surface reduce resistance to adsorbed molecules and thus facilitate their diffusion from model oil onto the adsorbent surface. A significant pore structure exists with a series of rocky structures distributed over the surface of DBT-loaded AgNPs^{cw}/AC.

The elemental composition of the blank ACB and Ag nanoparticles-modified ACs was obtained by energy dispersive X-ray analysis (EDX) (Fig. 5). It was found that the Ag nanoparticles-modified ACs have higher oxygen content compared to blank ACB due to the availability of oxygenated functional groups on the Ag nanoparticles-modified ACs surface. In addition the Ag nanoparticles-modified ACs show the traces of impregnated Ag with percent silver contents of 0.5 and 3.5% for AgNPs^{kp}/AC and AgNPs^{cw}/AC respectively. The raw activated carbon was not demineralized, and this accounts for the presence of high load of active metals in all the adsorbents (Fig. 5), which may also influence the DBT adsorption due to bond formation reaction between sulfur atom and these metals.

The energy dispersive spectrum (EDX) of AgNPs^{cw}/AC before and after adsorption of DBT showed the presence of 21.5% and 17.2% oxygen; 3.5% and −0.05% Ag, 6.2% and 40.3% carbon, respectively, in the blank and DBT loaded AgNPs^{cw}/AC. The increase in percentage carbon content and decrease in percentage oxygen content of DBT loaded AgNPscw/AC might be due to DBT loading or *n*-heptane sorption.

3.1.4. X-ray diffraction (XRD) analysis

Fig. 6 shows the XRD patterns of ACB, AgNPs^{kp}/AC, AgNPs^{cw}/AC and DBT loaded AgNPs^{cw}/AC. The XRD pattern of ACB shows two prominent peaks at 2θ values of 75.4°, 69.3°, which can be assigned to potassium oxide (K_2O). The AgNPs^{kp}/AC shows one strongest peak at 29.7°, which can be assigned to silver oxide (Ag_2O), while AgNPs^{cw}/AC shows three strongest peaks at 78.1°, 70.3° and 36.2°. The peak at 36.2° can be assigned to (Ag_2O) while peaks at 78.1° and 70.3° can be assigned to K_2O. The XRD patterns of AgNPs^{kp}/AC and AgNPs^{cw}/AC confirm that the ACB surface was successfully loaded by Ag nanoparticles. Also, all the peaks that appeared on the blank AgNPs^{cw}/AC have disappeared on the XRD of DBT loaded AgNPs^{cw}/AC. The disappearance can be due to elution of nanoparticles from AC surface or *n*-heptane sorption. An amorphous peak was also observed for all the adsorbents at 2θ value of 12.1°, which can be due to activated carbon.

3.2. Batch equilibrium studies

3.2.1. Effect of contact time

Fig. 7 shows the effect of contact time on the adsorption capacity of DBT from model oil by the adsorbents. It was observed that DBT adsorption from model oil by these adsorbents was rapid for the first 10 min on each type of adsorbents, and thereafter proceeded at a slower rate. The uptake of DBT was found to be 80–90% at 10–20 min. The initial rapid uptake capacity of the adsorbents may be due to large number of vacant sites available at the initial stage with subsequent resistance to occupation of the remaining vacant sites due to increased concentration gradient between the DBT molecules in the solution and DBT molecules in the adsorbent [40]. In addition, DBT is adsorbed from model oil into the pores which get almost saturated with DBT during initial stage of adsorption. Thereafter, the DBT molecules diffuse further and deeper into the micropores where they encounter much larger resistance resulting to slower rate of sorption process which naturally reached saturation during later period of adsorption.

The AgNPs^{kp}/AC and AgNPs^{cw}/AC exhibit higher adsorption capacities for DBT with maximum values of 25.7 and 29.8 mg $_{DBT}$/g_{Ads} at 25 °C respectively, than ACB with 13.9 mg $_{DBT}$/g_{Ads}. Table 2 compares the adsorption capacities of different adsorbents used in the adsorption of DBT from model oil, it was found out that the use

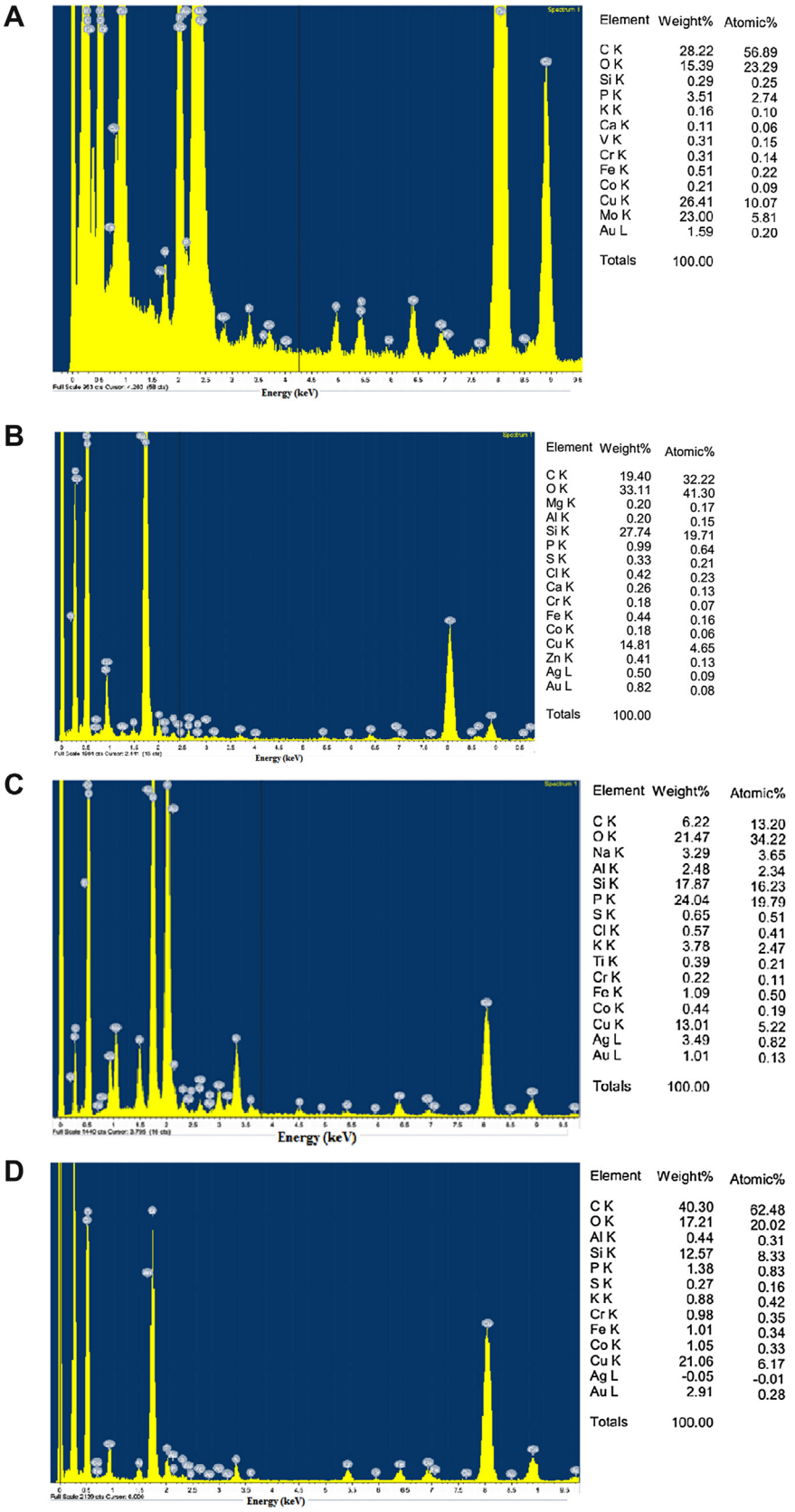

Fig. 5. Energy-dispersive X-ray (EDX) spectra of ACB (A), AgNPs^{kp}/AC (B), AgNPs^{cw}/AC(C) and DBT-loaded AgNPs^{cw}/AC (D).

of Ag nanoparticles-modified ACs from brewer's spent grains provides a better alternative for adsorptive desulphurization process. The AgNPs-modified activated carbon reported in the present study ranked moderately higher when compared with adsorbents that were recently reported by some authors, for example by [32], and comparable with SBA-16 reported by [9], but

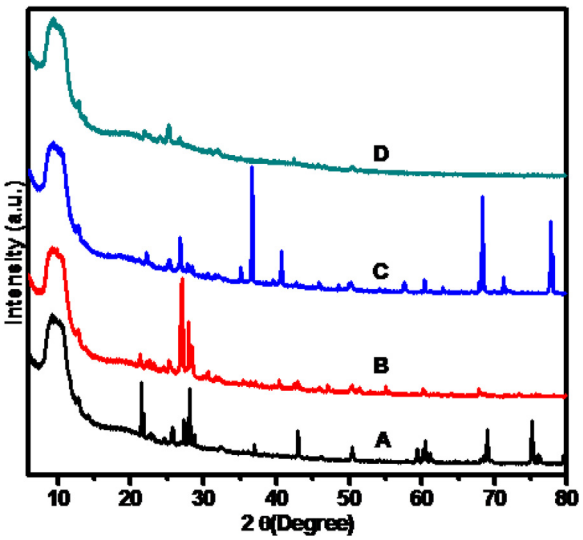

Fig. 6. Powder X-ray diffraction patterns of ACB (A), AgNPs^{kp}/AC (B), AgNPs^{cw}/AC (C) and AgNPs^{cw}/AC/DBT (D).

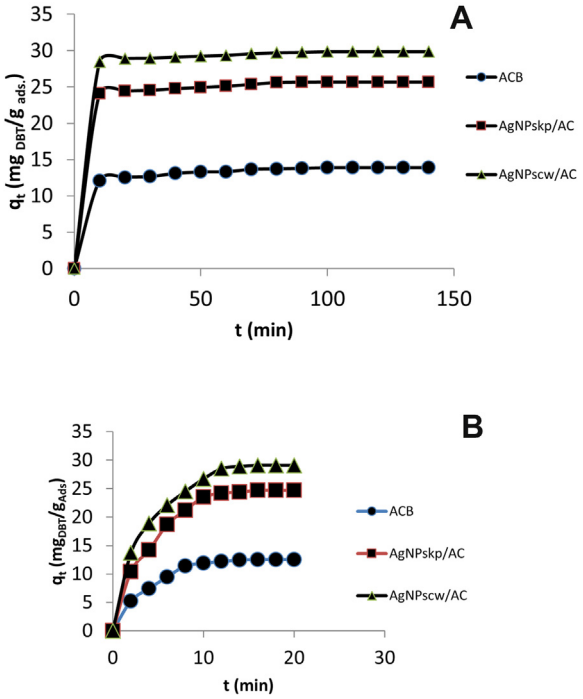

Fig. 7. The effect of contact time after 140 min (A) and in the first 20 min (B) on the adsorption capacity of DBT from model oil by the adsorbents.

lower in adsorption capacity for DBT than those recently reported by some authors, for example, [61] (Table 2).

The two-fold enhancement in the uptake capacities of Ag nanoparticles- modified ACs can be attributed to strong acid–base interaction between Ag(1) ion on the surface of the adsorbent and DBT. Therefore, the increase in the adsorption of DBT from model oil using Ag nanoparticles-modified ACs could be as a consequence of introducing an additional acidic adsorption sites on the surface of activated carbon which led to higher intensity of interaction of DBT with silver nanoparticles-modified activated carbon. Thiophenic compounds are known to interact with metal either via donation of a lone pairs of electron on sulphur forming a direct S-M $\sigma - bond$ or via delocalization of π-electrons of aromatic ring forming π-type complex with metals [69,79]. Because of the low reduction potential of silver, the silver species are likely to exist on dissolution or exposure to air as Ag^+ and Ag^0 with majority being Ag^+ [17]. The oxidized silver metal possibly form complex with DBT via S–Ag $\sigma - bond$, and thus causes strong adsorption of DBT on the surface of activated carbon [79]. The possible interaction between electron donor group containing sulfur such as DBT and Ag(1) ion on the surface of AgNPs/AC is illustrated in Fig. 8.

3.2.2. Effect of initial DBT concentration/adsorbent dose ratio

The effect of DBT concentration on the adsorption of DBT from model oil by the adsorbents was studied by varying initial DBT concentration range of 100–600 mg/L at adsorbent dose of 300 mg; while the effect of adsorbent dose was studied by varying adsorbent dose from 100 to 500 mg at initial DBT concentration of 400 mg/L. Both effects were studied at 298 K. The adsorption of DBT from model oil on all the adsorbent was found to increase with increasing DBT concentration and adsorbent dosage, where the adsorption of DBT in both cases became low after DBT concentration of 500 mg/L ($C_o > 500$ mg/L) and adsorbent dose of 400 mg ($m > 400$ mg). The increase in the percentage of DBT adsorbed with an increase in the adsorbate concentration is due to increase in mass transfer driving force resulting from concentration gradient developed between the bulk solution and surface of the adsorbent [8]; while the increase in DBT adsorption with increasing adsorbent dose may be attributed to increasing availability and accessibility of surface area and adsorption sites for the adsorption of DBT from model oil [21,4].

The strong relationship between the effect of initial DBT concentration and adsorbent dose was explored by studying the effect of DBT concentration/adsorbent dose ratio on the uptake of DBT from model oil using initial DBT concentration range 100–500 mg/L and adsorbent dose range of 100–500 mg (Fig. 9). As can be seen from the figure, the DBT uptake increases as the ratio increases, and became low after DBT concentration/adsorbent dose ratio of 4.0 ($r > 4.0$).

3.3. Adsorption isotherms of DBT

Fig. 10 shows the adsorption isotherms, q_e versus C_e at 25 °C for the adsorption of DBT on the adsorbents. It was found that the adsorption of DBT increases with increasing adsorbate concentrations. This might be due to hydrophobic nature of *n*-heptane, which is strongly adsorbed by AC, thereby influencing the removal of DBT from model oil. However, at low concentrations, there was sharp rise in q_e while at higher values of C_e, the increase in q_e became gradual. The non-linearity of the isotherms also confirms the competitive adsorption of DBT for the adsorption sites of the adsorbents [57].

The isotherm constants for the three isotherms studied, and the coefficient of determination, R^2 were determined from the experimental data using the linearized form of the three models and are listed in Table 3. The goodness of fit values, (R^2) for Freundlich are closer to unity in comparison to values obtained for the other two isotherms, and also the normalized standard deviation, Δq_e values are least for the fit of Freundlich isotherm. This indicates complexity of adsorption process with multilayer adsorption predominating.

The values of 1/n for the three adsorbents are greater than unity, which is indicative of cooperative adsorption [25,2], and not a normal Langmuir isotherm, where the 1/n value are below unity [25,2]. Also, since 1/n is greater than unity, the adsorption of DBT from model oil by these adsorbents is a chemical process involving adsorbate–adsorbent interactions [23]. The K_F values for modified adsorbents is higher than that of unmodified adsorbents, which

Table 2
Comparison of adsorption capacities of DBT from model oil on different adsorbents.

Adsorbent	Model oil	Adsorption capacity (mg/g)	References
CP(m)/MIL100(Fe)	*n*-Octane	110	[31]
Modified Zeolite	*n*-Hexane	109	[22]
D-MIP/CMSs[a]	*n*-Hexane	105.0	[51]
ACAL5[b]	*n*-Hexane	84.5	[59]
Fe_3O_4@-SiO_2@MIP	*n*-Octane	63.3	[48]
OMC[c]	*n*-Hexane	50.32	[9]
ACWS[d]	*n*-Heptane	47.1	[80]
AC-MnO_2	*n*-Heptane	43.2	[3]
CNTAL5[e]	*n*-Hexane	40.6	[59]
Ag-MCM–41[f]	*n*-Decane	32.6	[61]
SBA–16[g]	*n*-Hexane	29.56	[9]
MCM–41[h]	*n*-Decane	25.4	[61]
Alumina	*n*-Hexane	21.02	[68]
ACFH-Cu(1)[i]	*n*-Hexane	19.0	[54]
PT-Ag-MASN[j]	*n*-Decane	15.0	[32]
ACFH[k]	*n*-Hexane	14.0	[54]
AC-Cu Y zeolite	*n*-Docane/toluene	5.0	[30]
MSN[l]	*n*-Decane	4.60	[61]
Cu-Y zeolite	*n*-Docane/toluene	2.0	[30]
Nanocrystaline NaY zeolite	*n*-Nonane	1.7	[72]
ACB	*n*-Heptane	13.9	This study
$AgNPs^{kp}$/AC	*n*-Heptane	25.7	This study
$AgNPs^{cw}$/AC	*n*-Heptane	29.8	This study

[a]Carbon microsphere modified with double molecularly imprinted polymer, [b]Activated carbon loaded with 5% aluminium in the form of aluminium oxide, [c]ordered mesoporous carbon, [d]Activated carbon treated with steam at 900 °C then washed by H_2SO_4,[e]Carbon nanotube loaded with aluminium in the form of aluminium oxide, [f]Silver-impregnated mesoporous silica, [g]mesoporous silica, [h]bulk form of mesoporous silica, [i]Activated carbon fiber thermally treated and modified with copper cation, [j]platinum treated-silver impregnated mesoporous aluminosilicate nanoparticles, [k]Activated carbon fiber thermally treated, [l]mesoporous silica nanoparticles.

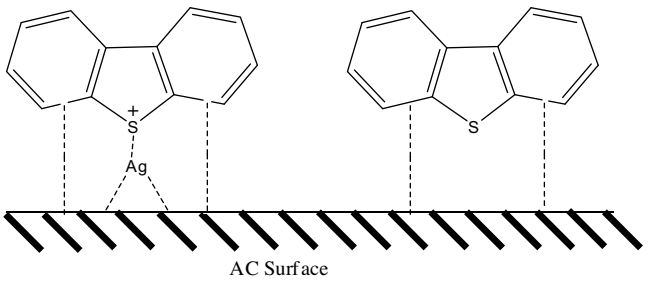

Fig. 8. Possible interactions of DBT molecules with blank and nano Ag/AC adsorbents.

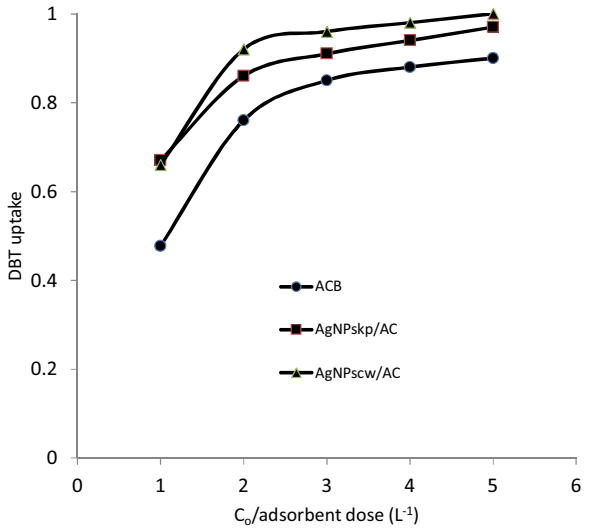

Fig. 9. Effect of initial DBT concentration/adsorbent dose on the uptake of DBT from model oil by the adsorbents at 298 K.

thus indicates higher adsorption capacity for DBT molecules compared to unmodified adsorbent.

The fundamental feature of Langmuir isotherm is expressed in terms of separation factor R_L. The R_L indicates isotherm to be either unfavorable $(R_L > 1)$, linear $(R_L = 1)$, favorable $(0 < R_L < 1)$ or irreversible $(R_L = 0)$. The R_L value for the adsorption of DBT from model oil by these adsorbents falls between 0 and 1, indicating that the adsorption was favorable (Table 3).

As shown in Table 3, the maximum adsorption capacity q_{max} for DBT on ACB, AgNPskp/AC and AgNPscw/AC follows the trend $AgNPs^{cw}$/AC > $AgNPs^{kp}$/AC > ACB.

The Temkin isotherm is usually used for the determination of energetic factor in the adsorption process. According to the results, DBT adsorption on $AgNPs^{cw}$/AC has the most exothermic energy (0.29 kJ/mol), thus suggesting that most favorable interaction occurs with this adsorbent from the thermodynamic point of view. However, the values of these energy factors seem relatively low (0.22–0.29 kJ/mol) which can be ascribed to the fact that the adsorption process deals with hydrophobic interactions which do not release energy as polar or ionic interactions, which is mainly due to dehydration/hydration behavior.

3.4. Kinetics of DBT adsorption

The study of the batch adsorption kinetics is essential for the design of industrial column [70]. In the present study, PFO, PSO and Elovich models have been tested to investigate the adsorption of DBT from model oil onto the adsorbents. The best-fit values of k_1, k_2, α, and β along with coefficient of determination (R^2) and $\Delta q_t(\%)$ for the PFO, PSO and Elovich models for DBT adsorption onto adsorbents with C_o(DBT) = 100 mg/L at 298 K is given in Table 4. According to the results, PSO kinetic model has the highest R^2 values and lowest normalized standard deviation, $\Delta q_t(\%)$ values. Therefore, the adsorption is best described by the PSO chemical reaction. It has been demonstrated that the PSO kinetic equation is much similar to the universal rate law for a chemical reaction [50]. Since the adsorption processes followed the PSO equation, it therefore suggests that the adsorption can be

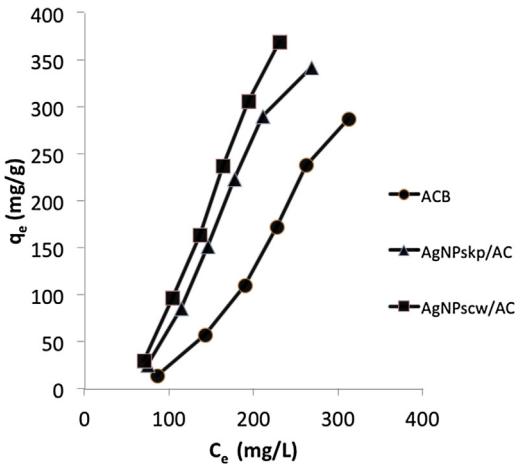

Fig. 10. Adsorption isotherms at 25 °C for DBT on the adsorbents. (C_0 = 100–600 mg/L, m = 300 mg).

Table 3
Isotherm parameters for the removal of DBT from model oil by the adsorbents (C_o(DBT) = 100–600 mg/L, m = 0.3 g, T = 298 K).

Isotherm model	Adsorbent		
	ACB	AgNPs^{kp}/AC	AgNPs^{cw}/AC
Langmuir			
$q_{max}(mg/g)$	33.1	63.3	71.9
$K_L x10^{-3}(L/mg)$	3.6	4.2	4.5
R^2	0.94	0.92	0.91
Δq_e	95	87	82
Freundlich			
$1/n$	2.4	2.1	2.1
$K_F x10^{-3}((mg/g)/(L/mg)^{1/n})$	0.4	3.2	4.5
R^2	0.99	0.97	0.97
Δq_e	12.2	21.6	15.9
Temkin			
$\beta(kJ/mol)$	0.22	0.27	0.29
$K_T x10^{-2}(L/mg)$	1.06	1.33	1.44
R^2	0.91	0.96	0.97
Δq_e	35.1	43.4	42.2

described by simple chemical interaction between the DBT molecules and the functional elements on surface of ACB, where the interaction was further enhanced by the presence of Ag(1) ion on the surface of Ag nanoparticles-modified ACs.

Table 4
Kinetic parameters for the removal of DBT from model oil onto the adsorbents (C_o(DBT) = 100 mg/L, m = 0.2 g, T = 298 K).

Model	Kinetic parameters	Adsorbents		
		ACB	AgNPs^{kp}/AC	AgNPs^{cw}/AC
PFO	$q_{e,exp.}(mg/g)$	12.6	24.7	29.1
	$q_{e,cal.}(mg/g)$	20.4	38.9	47.6
	$k_1 x10^{-1}(min^{-1})$	3.6	3.4	3.5
	R^2	0.97	0.98	0.93
	$\Delta q_t(\%)$	55.5	53.2	50.6
PSO	$q_{e,cal.}(mg/g)$	16.4	32.2	37.0
	$k_2 x10^{-3}(g/mg.min)$	15.0	7.2	7.5
	R^2	0.99	0.99	1.0
	$\Delta q_t(\%)$	37.7	38.4	31.7
Elovich	$\alpha(mg/g.min)$	7.7	14.8	22.5
	$\beta(mg/g)$	0.26	0.13	0.13
	R^2	0.97	0.97	0.99
	$\Delta q_t(\%)$	93.5	97.2	98.1

3.5. Adsorption thermodynamics

Thermodynamic parameters for the adsorption of DBT from model oil by ACB, AgNPs^{kp}/AC and AgNPs^{cw}/AC are obtained from the plot of InK_L^r against $1/T$(Fig. 11), and are given in Table 5. The positive values of ΔH^oshow that the adsorptive desulphurization process is endothermic in nature. The adsorption of DBT from model oil was feasible and spontaneous at all the temperatures investigated as indicated from the negative values of ΔG^o. The positive value of ΔS^o suggests increased randomness of the DBT molecules on the solid surface than in the solution.

3.6. Adsorption mechanism

The influence of mass transfer resistance on binding of DBT on the adsorbents was verified by exploring Weber and Morris intra-particle diffusion resistance model using Eq. (12) [78].

Fig. 12 shows plots of q_t versus $t^{0.5}$for adsorption of DBT on ACB, AgNPs^{kp}/AC and AgNPs^{cw}/AC at 25 °C. These results imply that the adsorption processes involve more than a single kinetic stage or sorption rate [78]. The first portion gives the diffusion of adsorbate through the solution to the external surface of adsorbent. The second linear portion is attributed to the equilibrium stage with intra-particle diffusion predominating. The presence of micropores on the adsorbents is in agreement with this stage (Table 6). When the linear portions are extrapolated back to the y-axis, they give intercepts which provide the measure of boundary layer thickness. The deviation of straight lines from origin (i.e. $C_i \neq 0$) indicates that intra-particle diffusion (pore diffusion) is not the sole rate-controlling step. Therefore, the adsorption proceeds via a complex mechanism [18] consisting of both surface adsorption and intra-particle transport within the pores of adsorbent. The slopes of the first plots (k_{id1}) are higher than that of the second linear plot (k_{id2}), which corresponds to an enhanced diffusion of DBT through meso- and micro pores as a result of greater driving force at higher C_o.

3.7. Regeneration studies

These were carried out by filtering the DBT-loaded AgNPs^{kp}/AC and AgNPs^{cw}/AC, followed by thermal treatment of the residue in the atmosphere at 450 °C for 6 h [83] to remove the adsorbed DBT molecules. The regenerated AgNPs^{kp}/AC and AgNPs^{cw}/AC were then re-used for the next adsorption, and this was repeated five times for the successive adsorption–desorption cycles. There was slight reduction in the adsorption capacity after the first regeneration (Fig. 13) with significant reduction in adsorption capacity after 5 successive regeneration cycles. The reduction in adsorptive capacity can be attributed to the deposition of

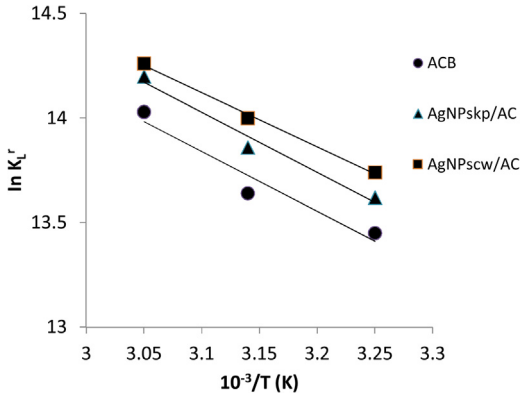

Fig. 11. Van't Hoff plot for the adsorption of DBT from model oil by the adsorbents.

Table 5
Thermodynamic parameters for the adsorption of DBT onto the adsorbents (C_o (DBT) = 200 mg/L, m = 0.3 g).

Adsorbent	R^2	ΔH^o (kJ/mol)	ΔS^o (kJ/molK)	$-\Delta G^o$ (kJ/mol)		
				308	318	328
ACB	0.936	23.75	0.19	34.8	36.7	38.6
AgNPs^{kp}/AC	0.975	23.89	0.19	34.6	36.5	38.4
AgNPs^{cw}/AC	0.996	21.54	0.18	33.9	35.7	37.5

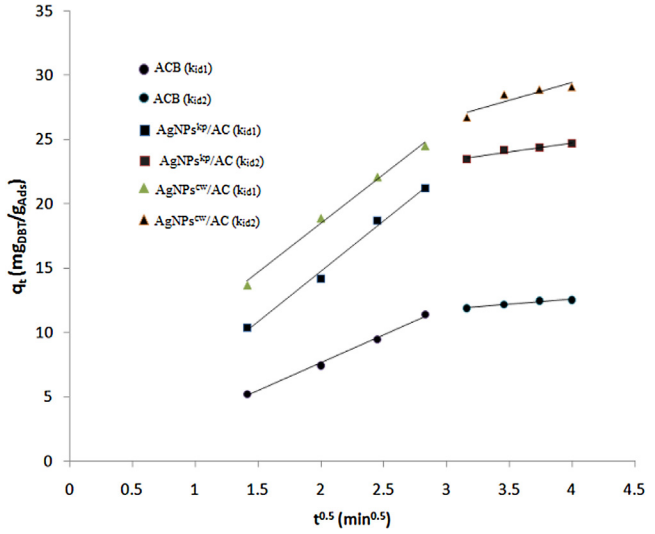

Fig. 12. Plots of q_t versus $t^{0.5}$ showing the two diffusion stages predicted by the diffusion model for the removal of DBT from model oil by the adsorbents. (C_o (DBT) = 100 mg/L, T = 298 K, m = 0.2 g).

Table 6
Intra-particle diffusion parameters for adsorption of DBT on different adsorbents (C_o = 100 mg/L, m = 0.2 g, T = 298 K).

Parameters	Adsorbents		
	ACB	AgNPs^{kp}/AC	AgNPs^{cw}/AC
K_{id1} (mg/g.min$^{1/2}$)	4.3	7.8	7.6
K_{id2} (mg/g.min$^{1/2}$)	0.8	1.4	2.8
C_1	−1.0	−0.9	3.2
C_2	9.4	19.3	18.4
$(R_1)^2$	1.0	0.99	0.99
$(R_2)^2$	0.97	0.94	0.82

decomposed products of the adsorbate-adsorbent interactions that occurred on the surface of the adsorbent. However, the adsorbent can still be used for at least 3 regenerative cycles with more than 80% adsorption capacity.

3.8. Adsorption of DBT from commercial gasoline sample

The potential application of using AgNPs^{cw}/AC which has the highest adsorption capacity among the prepared adsorbents was evaluated for DBT removal from commercial gasoline by measuring the DBT concentration before and after the adsorption based on the standard addition method. A commercial gasoline was purchased from NNPC depot from Ilorin, Kwara State, Nigeria. A GC-PFPD chromatogram (HP 6890 model) of the commercial gasoline with identification of major peaks is shown in Fig. 14. The major sulphur compounds existing in the commercial gasoline of the present study are mercaptan, thiophene, benzothiophene, dibenzothiophene, 4-methyldibenzothiophene, 4,6-dimethyldibenzothiophene and dibenzyldisulphide. The DBT concentration in the commercial gasoline was very small (5.09 mg/L), and in order to check the effectiveness of this adsorbent for DBT removal at higher concentration, a real gasoline sample was spiked with DBT of known concentration to increase its concentration in the original gasoline sample to 115.6 mg/L. The adsorption result at optimum adsorbent dosage of 400 mg shows that the DBT concentration was reduced to 79.2 mg/L with removal percentage of about 31.5%. This relatively low removal efficiency at the optimum adsorbent dosage of 400 mg could be attributed to the complexity of the medium of a real gasoline sample which contains other competing aliphatic sulphur compounds such as mercaptan and aromatic sulfur compounds. Also, the solubility of DBT in these medium is enhanced due to the aromatic nature of the complex gasoline medium, and its diffusion to the adsorbent surface would be very low compared with its diffusion in the model oil of single component (*n*-heptane alone) used in this study.

4. Conclusion

The present study shows that Ag nanoparticles-modified AC is a promising adsorbent for desulphurization of liquid fuels. The presence of DBT on the surface of the adsorbent was confirmed by comparing the physicochemical characteristics of the blank AgNPs^{cw}/AC with that of the DBT loaded AgNPs^{cw}/AC. Kinetic study for adsorbent has shown that the best fit is achieved with PSO equation. Equilibrium data were best described by the Freundlich isotherm model. The adsorption of DBT onto these adsorbents was found to be endothermic in nature, feasible and

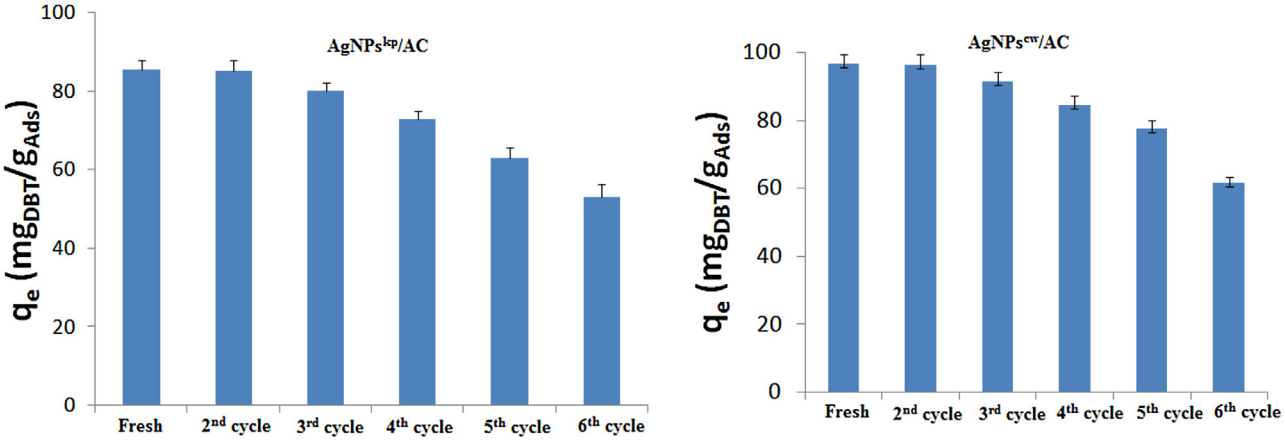

Fig. 13. The adsorption capacities with error bars after 5 successive adsorbent regeneration cycles for DBT on AgNPs^{kp}/AC adsorbent and DBT on AgNPs^{cw}/AC adsorbent.

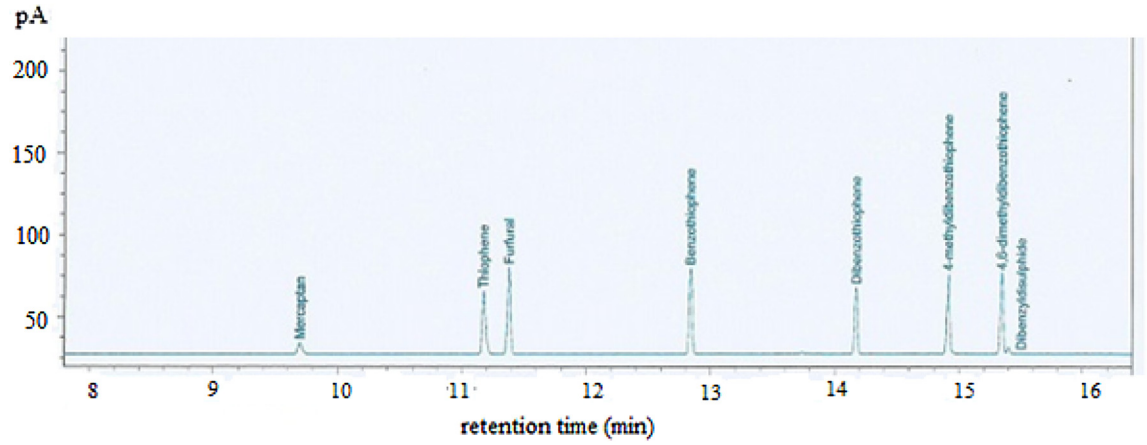

Fig. 14. GC-PFPD chromatogram of commercial gasoline.

spontaneous. Our results both in terms of adsorption capacity and surface modifications indicate that Ag nanoparticles-modified AC will find useful applications in petroleum industry because of its simplicity, eco-friendliness and high efficiency.

Conflict of interest

There are no competing interests.

Acknowledgement

All thanked Technologists of Research Centre of the University of KwaZulu-natal, South Africa for their technical assistance.

References

[1] R. Abdul, Z. Yacob, M. Abdul, S. Ratna, D. Dewi, I. Vincinisvarri, Comparison of various sources of high surface area activated carbons prepared by different types of activation, Malays. J. Anal. Sci. 1 (1) (2008) 12–18.
[2] A. Abia, E.D. Asuquo, Lead (II) and nickel (II) adsorption kinetics from aqueous metal solutions using chemically modified and unmodified agricultural adsorbents, Afr. J. Biotechnol. 5 (16) (2006) 1475–1482.
[3] K.A. Abu Safieh, Y.S. Al-Degs, M.S. Sunjuk, A.I. Saleh, M.A. Al-Ghouti, Selective removal of dibenzothiophene from commercial diesel using manganese dioxide-modified activated carbon: a kinetic study, Environ. Technol. (2014), doi:http://dx.doi.org/10.1080/09593330.2014.938125.
[4] A.A. Adeyi, I.T. Popoola, A.S. Yusuff, A.S. Olateju, Kinetics analysis and dosage effect of manganese dioxide adsorbent on desulphurization of crude oil, J. Bioprocess. Chem. Eng. 2 (2014) 1–6.
[5] C. Aharoni, M. Ungarish, Kinetics of activated chemisorption. Part 1. The Non-Elovich Part of the isotherm, J. Chem. Soc. Farad. Trans. 72 (1976) 265–268.
[6] W. Ahmad, I. Ahmad, M. Ishaq, K. Ihsan, Adsorptive desulfurization of kerosene and diesel oil by Zn impregnated montmorollonite clay, Arabian J. Chem. (2014), doi:http://dx.doi.org/10.1016/j.arabjc.2013.12.025.
[7] I.A.H. Al Zubaidy, F.B. Tarsh, N.N. Darwish, B.S.S. Abdul Majeed, A. Al Sharafi, L. A. Chacra, Adsorption process of sulfur removal from diesel oil using sorbent materials, J. Clean Energy Technol. 1 (1) (2013) 66–68.
[8] M. Anbia, Z. Parvin, Desulphurization of fuel by means of nanoporous carbon adsorbent, Chem. Eng. Res. Dev. 89 (2011) 641–647.
[9] M. Anbia, S. Karami, Desulphurization of gasoline using novel mesoporous carbon adsorbents, J. Nanostruct. Chem. 5 (2015) 131–137.
[10] C.O. Ania, T.J. Bandosz, Metal-loaded polystyrene-based activated carbons as dibenzothiophene removal media via reactive adsorption, Carbon 44 (2006) 2404–2412.
[11] M. Arami, N.Y. Limace, N.M. Mahmoodi, N.S. Tabrizi, Equilibrium and kinetics studies for the adsorption of direct and acid dyes from aqueous solution by soy meal hull, J. Hazard. Mater. B 135 (2006) 171–179.
[13] P. Baltzopoulou, K.X. Kallis, G. Karagiannakis, A.G. Konstandopoulos, Diesel fuel desulphurization via adsorption with aid of activated carbon: laboratory- and pilot scale studies, Energy Fuels 29 (9) (2015) 5640–5648.
[14] S.K. Bej, S.K. Maity, U.T. Turaga, Search for an efficient 4,6-DMDBT hydrodesulfurization catalyst: a review of recent studies, Energy Fuels 18 (2004) 1227–1237.
[15] S.K. Behzad, A. Balati, M.M. Amini, M. Ghanbari, Triazine-modified magnetic nanoparticles as a novel sorbent for preconcentration of lead and cadmium ions, Microchim. Acta 181 (15) (2014) 1781–1788.
[16] J. Bu, G. Loh, C.G. Gwie, S. Dewiyanti, M. Tasrif, A. Borgna, Desulphurization of diesel fuels by selective adsorption on activated carbons: competitive adsorption of polycyclic aromatic sulphur heterocycles and polycyclic aromatic hydrocarbons, Chem. Eng. J. 166 (2011) 207–217.
[17] I. Capek, Plasmonic nanoparticles and their conjugates: preparation, optical properties and antimicrobial activity, J. Nanotechnol. Mater. Sci. 2 (1) (2015) 1–18.
[18] A.K. Chaturvedi, K.C. Pathak, V.N. Singh, Fluoride removal from water by adsorption on china clay, Appl. Clay Sci. 3 (1988) 337–346.
[20] M.J. da Silva, L.F. dos Santos, Novel oxidative desulfurization of a model fuel with H_2O_2 catalyzed by $AlPMo_{12}O_{40}$ under phase transfer catalyst-free conditions, J. Appl. Chem. (2013), doi:http://dx.doi.org/10.1155/2013/147945.
[21] N. Dizge, C. Aydiner, E. Demirbas, M. Kobya, S. Kare, Adsorption of reactive dyes from aqueous solution by fly ash: kinetic and equilibrium studies, J. Hazard. Mater. 150 (2008) 737–746.
[22] H. Faghihian, M. Yahyaie, Removal of dibenzothiophene from organic medium by modified zeolite, J Chem. Petroleum Eng. 47 (2) (2013) 107–114 (University of Tehran).
[23] A.M. Farhan, H.A. Al-Dujaili, M.A. Awwad, Equilibrium and kinetic studiesofcadmium (II) and lead (II) ions biosorption onto *Ficus carcia* leaves, Int. J. Ind. Chem. 4 (2013) 24–31.
[24] H.M.F. Freundlich, Over the adsorption in solution, J. Phys. Chem. 57 (1906) 385–471.
[25] K. Fytianos, E. Voudrias, E. Kokkalis, Sorption desorption behaviour of 2,4-dichlorophenol by marine sediments, Chemosphere 40 (2000) 3–6.
[26] U. Garg, M.P. Kaur, G.K. Jawa, D. Sudi, V.K. Garg, Removal of cadmium (II) from aqueous solutions by adsorption on agricultural waste biomass, J. Hazard. Mater. 154 (2008) 1149–1157.
[27] P. Gawande, J. Kaware, Review on low cost adsorbents for desulphurization of liquid fuels, IJSRSET 2 (1) (2016) 108–112.
[28] E. Gomez, V.E. Santos, A. Alcon, A.B. Martin, F. Garcia-Ochoa, Oxygen-uptake and mass transfer rates on the grown of pseudomonas putida CECT5279: Influence on biodesulphurization, (BDS) capability, Energy Fuels 20 (4) (2006) 1565–1571.
[29] Y. Guoxian, C. Hui, L. Shanxiang, Z. Zhongnan, Deep desulphurization of diesel by catalytic oxidation, Chem. Eng. China 1 (2) (2007) 162–166.
[30] N.M. Hadi, S.A. Rashi, S. Abdalreda, Deep desulfurization of diesel fuel by guard bed adsorption of activated carbon and locally prepared Cu-Y zeolite, J. Eng. 20 (5) (2014) 146–159.
[31] Z. Hasan, S.H. Jhung, A facile method to disperse non-porous metal organic frameworks: composite formation with a porous metal organic framework and application in adsorptive desulfurization, ACS Appl. Mater. Interfaces 7 (19) (2015) 10429–10435.
[32] J.L. Hauser, D.T. Tran, E.T. Conley, J.M. Saunders, K.C. Bustillo, S.R.J. Oliver, Plasma treated of silver impregnated mesoporous aluminosilicate nanoparticles for adsorptive desulphurization, Chem. Mater. 28 (2) (2016) 474–479.
[34] Y.S. Ho, G. McKay, Pseudo-second order model for sorption processes, Process Biochem. 34 (1999) 451–465.
[35] International Union of Pure and Applied Chemistry (IUPAC), Manual of Symbols and Terminology for Physico-chemical Quantities and Units, Appendix II. Part I. Definitions,terminology and symbols in colloid and surface chemistry, Pure Appl. Chem. 31 (1972) 579–638.
[36] M. Ishaq, S. Sultan, I. Ahmad, H. Ullah, M. Yaseen, A. Amir, Adsorptive desulphurization of model oil using untreated, acid activated and magnetite nanoparticles loaded bentonite as adsorbent, J. Saudi Chem. Soc. (2015) 1–9.
[37] D. Jayne, Y. Zhang, S. Haji, C. Erkey, Dynamics of removal of organosulfur compounds from diesel by adsorption on carbon aerogels for fuel cell applications, Int. J. Hydrogen Energy 30 (2005) 1287–1293.
[38] Z. Jiang, H. Lü, Y. Zhang, C. Li, Oxidative desulfurization of fuel oils, Chin. J. Catal. 32 (2011) 707–715.

[39] X. Jiang, Y. Nie, C. Li, Z. Wang, Imidazolium-based alkyl phosphate ionic liquids—a potential solvent for extractive desulphurization of fuel, Fuel 8 (7) (2008) 79–84.
[40] D. Kavitha, C. Namasivayam, Recycling coir pitch, an agricultural solid waste for the removal of procion orange from wastewater, Dyes Pigments 74 (2007) 237–248.
[42] E. Kianpour, S. Azizian, Optimization of dispersed carbon nanoparticles synthesis for rapid desulphurization of liquid fuel, Pet. Sci. 13 (2016) 146–154.
[43] M. Komarneni, E. Kadossov, J. Justin, M. Lu, U. Burghaus, Adsorption of thiophene on silica-supported Mo clusters, Surf. Sci. 604 (2010) 1221–1229.
[44] S. Lagergren, Zur theorie der sogenannten adsorption gelo ster stoffe Kungliga. Svenska vetenskapsakademiens 24 2 1898; 1–39.
[45] I. Langmuir, The adsorption of gases on plane surfaces of glass, mica, and platinum, J. Am. Chem. Soc. 40 (1918) 1361–1403.
[46] A. Lateef, S.A. Ojo, M.A. Azeez, T.B. Asafa, T.A. Yekeen, A. Akinboro, I.C. Oladipo, E.B. Gueguim-Kana, L.S. Beukes, Cobweb as novel biomaterial for green and eco-friendly synthesis of silver nanoparticles, Appl. Nanosci. 6 (2016) 863–874.
[47] A. Lateef, M.A. Azeez, T.B. Asafa, T.A. Yekeen, A. Akinboro, I.C. Oladipo, L. Azeez, S.E. Ajibade, S.A. Ojo, E.B. Gueguim-Kana, L.S. Beukes, Biogenic synthesis of silver nanoparticles using a pod extract of *Cola nitida*: antibacterial, antioxidant activities and application as a paint additive, J. Taibah Univ. Sci. 10 (4) (2016) 551–562.
[48] H. Li, W. Xu, N. Wang, X. Ma, D. Niu, B. Jiang, L. Liu, W. Huang, W. Yang, Z. Zhou, Synthesis of magnetic molecularly imprinted polymer particles for selective adsorption and separation of dibenzothiophene, Microchim. Acta 179 (2012) 123–130.
[49] H. Liu, J. Yu, X. Bao, The State-of-the-art and future perspectives of world petroleum refining technology, Chin. J. Process Eng. 7 (1) (2007) 176–185 (in Chinese).
[50] Y. Liu, New insight to pseudo second-order kinetic equation foradsorption, Colloid Surf. A 320 (2008) 275–278.
[51] W. Liu, X. Liu, Y. Yang, Y. Zhang, B. Xu, Selective removalof benzothiophene and dibenzothiophene from gasoline usingdouble-template molecularly imprinted polymers on the surface ofcarbon microspheres, Fuel 117 (2014) 184–190.
[52] X. Ma, M. Sprague, C. Song, Deep desulfurization of gasoline by selective adsorption over nickel-based adsorbent for fuel cell applications, Ind. Eng. Chem. Res. 44 (2005) 5768–5775.
[53] S.K. Milonjic, A consideration of the correct calculation of thermodynamic parameters of adsorption, J. Serb. Chem. Soc. 72 (12) (2007) 1363–1367.
[54] E.S. Moosavi, S.A. Dastgheib, R. Karimzadeh, Adsorption of thiophenic compounds from model diesel fuel using copper and nickel impregnated activated carbons, Energies 5 (2012) 4233–4250.
[55] A. Masoumi, K. Hemmati, M. Ghaemy, Low-cost nanoparticles sorbent from modified rice husk and a copolymer for efficient removal of Pb(II) and crystal violet from water, Chemosphere 146 (2016) 253–262.
[56] A. Mirabi, Z. Dalirandeh, A.S. Rad, Preparation of modified magnetic nanoparticles as a sorbent for preconcentration and determination of cadmium ions in ood and environmental water samples prior to flame atomic absorption spectrometry, J. Magnetism Magn. Mater. 381 (2015) 138–144.
[57] A.E. Navarro, R. Portales, R. Sun-Kou, B.P. Llanos, Effect of pH on phenol biosorption by marine seaweeds, J. Hazard. Mater. 156 (2008) 405–411.
[59] M.K. Nazal, M. Khaled, M.A. Atieh, I.H. Aljundi, G.A. Oweimreen, A.M. Abulkibash, The nature and kinetics of the adsorption of dibenzothiophene in model diesel fuel on carbonaceous materials loaded with aluminumoxide particles, Arabian J. Chem. (2015), doi:http://dx.doi.org/10.1016/j.arabjc.2015.12.003.
[60] J.G. Park, C.H. Ko, K.B. Yi, J.H. Park, S.S. Han, S.H. Cho, J.N. Kim, Reactive adsorption of sulfur compounds in diesel on nickel supported on mesoporous silica, Appl. Catal. B 81 (2008) 244–250.
[61] J.M. Palomino, D.T. Tran, J.L. Hauser, H. Dong, S.R.J. Oliver, Mesoporous silica nanoparticles for high capacity adsorptive desulfurization, J. Mater. Chem. A 2 (2014) 14890–14895.
[62] D. Peralta, G. Chaplais, A. Simon-Masseron, K. Barthelet, G.D. Pirngruber, Metal-organic framework materials for desulfurization by adsorption, Energy Fuels 26 (8) (2012) 4953–4960, doi:http://dx.doi.org/10.1021/ef300762z.
[63] H.R. Rajabi, H. Arjmand, S.J. Hoseini, H. Nasrabadi, Surface modified magnetic nanoparticles as efficient and green sorbents: synthesis, characterization and application for the removal of anionic dye, J. Magnetism Magn. Mater. 394 (2015) 7–13.
[65] A. Rothlisberger, R. Prins, Intermediates in the hydrodesulphurization of 4,6-dimethyl- dibenzothiophene over Pd/γ-Al_2O_3, J. Catal. 235 (2005) 229–240.
[66] M. Shakirullah, A.I. Imtiaz, A.W. Waqas, I.M. Mohammad, Desulphurization study of petroleum products through extraction with aqueous ionic liquids, J. Chil. Chem. Soc. 55 (2) (2010) 179–183.
[67] M. Seredych, C.T. Wu, P. Brender, C.O. Ania, C. Vix-Guterl, T.J. Bandosz, Role of phosphorus in carbon matrix in desulphurization of diesel fuel using adsorption process, Fuel 92 (2012) 318–326.
[68] A. Srivastav, V.C. Srivastava, Adsorptive desulfurization by activated alumina, J. Hazard. Mater. 170 (2009) 1133–1140.
[69] C. Song, An overview of new approaches to deep desulphurization for ultra-clean gasoline, diesel fuel and jet fuel, Catal. Today 11 (2003) 211–263.
[70] C. Song, X. Ma, New design approaches to ultra-clean diesel fuels by deep desulfurization and deep dearomatization, Appl. Catal. B 41 (2003) 207–238.
[71] X.U. Tao, L. Xiaoqin, Peanut shell activated carbon: Characterization, surface modification and adsorption of Pb^{2+} from aqueous Solution, Chin. J. Chem. Eng. 19 (3) (2008) 401–406.
[72] K. Tang, X. Hong, Y. Zhao, Y. Wang, Adsorption desulphurization on a nanocrystalline NaY zeolite synthesized using carbon nanotube template growth, Pet. Sci. Technol. 29 (2011) 779–787.
[73] M.I. Temkin, V. Pyzhev, Kinetics of ammonia synthesis on promoted iron catalysts, Acta Physiochim. URSS 12 (1940) 327–356.
[74] S. Tokalioglu, F. Gurbuz, Selective determination of copper and iron in various food samples, Food Chem. 123 (2010) 183–187.
[75] M. Tymchyshyn, Deep Desulphurization of Diesel Fuels, Lakehead University, 2008.
[76] J. Wang, F. Xu, W. Xie, Z. Mei, Q. Zhang, J. Cai, W. Cai, The enhanced adsorption of dibenzothiophene onto cerium/nickel-exchanged zeolite Y, J. Hazard. Mater. 163 (2009) 538–543.
[77] Y. Wang, X. Luo, J. Tang, X. Hu, Q. Xu, C. Yang, Extraction and preconcentration of trace levels of cobalt using functionalized magnetic nanoparticles in a sequential injection lab-on-valve system with detection by eelectrothermal atomic absorption spectrometry, Anal. Chim. Acta 713 (2012) 92–96.
[78] W.J. Weber, J.C. Morris, Kinetics of adsorption on carbon from solution, J. Sanit. Eng. Div. Am. Soc. Eng. 89 (1963) 31–60.
[79] X. Yang, L.E. Erickson, K.L. Hohn, P. Jeevanandam, K.L. Klabunde, Sol-gel Cu-Al_2O_3 adsorbents for selective adsorption of thiophene out of hydrocarbon, Ind. Eng. Chem. Res. 45 (2006) 6169–6174.
[80] Y. Yang, H. Lu, P. Ying, Z. Jiang, C. Li, Selective dibenzothiophene adsorption on modified activated carbons, Carbon 45 (2007) 3042–3044.
[81] S. Yosuke, S. Kazuom, C. Ki-Hyouk, K. Yozo, M. Isao, Two step adsorption process for deep desulphurization of diesel oil, Fuel 84 (7–8) (2005) 903–910.
[82] C. Yu, J.S. Qiu, Y.F. Sun, X.H. Li, G. Chen, Z. Bin, Adsorption removal of thiophene and dibenzothiophene from oils with activated carbon as adsorbent: effect of surface chemistry, J. Porous Mater. 15 (2008) 151–157.
[83] Z.Y. Zhang, T.B. Shi, C.Z. Jia, W.J. Ji, Y. Chen, M.Y. He, Adsorptive removal of aromatic organosulfur compounds over the modified Na-Y zeolites, Appl. Catal. B 82 (2008) 1.
[84] Ma Zhao, C. Song, Liquid-phase adsorption of multi-ring thiophene sulphur compounds on carbon materials with different surface properties, J. Phys. Chem. B 110 (10) (2006) 4699–4707.
[85] X. Zhao, J. Wang, F. Wu, T. Wang, Y. Cai, Y. Shi, G. Jiang, Removal of fluoride from aqueous media by Fe_3O_4@$Al(OH)_3$ magnetic nanoparticles, J. Hazard. Mater. 173 (2010) 102–109.
[86] A. Zhou, X. Ma, C. Song, Effects of oxidative modification of carbon surface on the adsorption of sulfur compounds in diesel fuel, Appl. Catal. B 87 (2009) 190–199.